

# Setting in motion and entraining a Herschel-Bulkley fluid

Christophe Ancey<sup>a,1</sup>, Belinda M. Bates<sup>a,1</sup>

<sup>a</sup>*Environmental Hydraulics Laboratory, École Polytechnique Fédérale de Lausanne, EPFL  
ENAC IIC LHE, Btiment GC (Station 18), CH-1015 Lausanne, Switzerland*

---

## Abstract

Herschel-Bulkley materials can be set in motion when a sufficiently high shear stress or body force is applied. We investigate the behaviour of a layer of Herschel-Bulkley fluid when suddenly tilted. The material's dynamic response depends on the details of its constitutive equation. When the rheological behaviour is viscoelastoplastic with no thixotropic behaviour, the material is set in motion instantaneously along its base. When the rheological behaviour involves two yield stresses (static and dynamic yield stresses), the material must be destabilised before it starts to flow. This problem is then similar to a Stefan problem, with an interface that separates sheared and unsheared regions and moves from top to bottom. In both these cases, the time needed to set the layer in motion is short when the layer is shallow. This makes it possible to assume that viscoplastic flows can erode shallow viscoplastic layers almost instantaneously. We show the consequences of this sudden incorporation of material on the motion of viscoplastic dambreak flows.

*Keywords:* Herschel-Bulkley fluids, Stokes problem, lubrication theory, shear flow

---

## 1. Introduction

Viscoplastic fluid theory has long been used to approximate the complex rheological behaviour of natural materials such as snow and mud, particularly

---

*Email address:* [christophe.ancey@epfl.ch](mailto:christophe.ancey@epfl.ch) (Christophe Ancey)

their transition between solid- and fluid-like states [1]. The theory's strength lies in its capacity to describe flow initiation and cessation using a single constitutive equation. Natural materials can also erode the bed on which they flow and, in this case, it is tempting to see bed erosion as a form of yielding induced by the passage of the flow [2–4].

Various processes are at work when bed materials are set in motion. Among these, two are expected to play a major part: the increase in the normal and shear stresses applied to the bed surface, and the decrease in the shear strength relative to gravitational forces. The first process is certainly the easiest to investigate experimentally and theoretically. The Stokes problem provides a theoretical perspective: fluid is set in motion by applying a shear stress to its boundary or by moving that boundary at a constant velocity [5, 6]. The second process can be studied by suddenly applying a body force to the fluid initially at rest. For convenience, this paper refers to this problem as Stokes' third problem. For Newtonian fluids, there exists a similarity solution to this problem, which shows that the fluid is instantaneously set in motion and virtually all the fluid layer is entrained even though the effects far from the boundary are exponentially small [6]. Compared to Newtonian fluids, the dynamic response of Herschel-Bulkley materials to a sudden change in the stress state is made more complex by their ability to remain static when the stress state lies below a certain threshold, and to yield when the stress state moves above it.

This paper investigates Stokes' third problem for Herschel-Bulkley fluids. More specifically, we aim to determine the characteristic time  $t_c$  associated with the setting in motion of a Herschel-Bulkley fluid suddenly experiencing a body force and/or a shear stress, as well as the features of the layer of fluid that is entrained. Time  $t_c$  is of particular relevance when determining the erosion rate of static viscoplastic layers or assessing the strength of the coupling between entrainment and flow. Indeed, if we consider that viscoplastic materials flow over a static viscoplastic layer, we can relate  $t_c$  to the flow timescale  $t_f$ . If  $t_c = O(t_f)$ , then the governing equations for the flow eroding its bed involve one equation for the evolution of the flow and another for describing bed dynamics, and they

are coupled. Otherwise, when  $t_c \ll t_f$ , yielding and entrainment are nearly instantaneous at the flow scale, and a single equation suffices to describe the bulk dynamics. This paper will give an example of an application by considering the motion of a viscoplastic avalanche entraining a shallow stationary layer made of the same fluid.

We begin by setting out what we refer to as Stokes' third problem (Sec. 2). We focus on Herschel-Bulkley fluids and outline the current state of the art in modelling Herschel-Bulkley fluids. Our literature review led us to consider two types of Herschel-Bulkley fluids: simple Herschel-Bulkley fluids, whose rheological behaviour is well described by a one-to-one constitutive equation, and non-simple Herschel-Bulkley fluids, whose rheological behaviour exhibits shear-history dependence. The details of the constitutive equation have a great deal of influence on the solution to Stokes' third problem. In Sec. 3, which is devoted to simple Herschel-Bulkley fluids, we show that the material is instantaneously set in motion. By contrast, non-simple Herschel-Bulkley materials do not start moving spontaneously; they must first be destabilised. A front subsequently propagates through the static layers and sets them in motion (Sec. 4). In Sec. 5, we study how the instantaneous entrainment of a shallow stationary viscoplastic layer affects the motion of a viscoplastic avalanche. The theoretical results are discussed in Sec. 6.

## 2. Stokes' third problem

The literature refers to two Stokes problems. Stokes' first problem refers to the impulsive motion of a semi-infinite volume of Newtonian fluid sheared by an infinite solid boundary. Stokes' second problem concerns the cyclical motion of this volume sheared by an oscillatory boundary [6]. These two problems have also been investigated for viscoplastic materials [7–9].

A related problem concerns the setting in motion of a layer of fluid of depth  $H$ , initially at rest and suddenly tilted at an angle  $\theta$  to the horizontal (see Fig. 1). Contrary to the two Stokes problems above, we consider a volume that

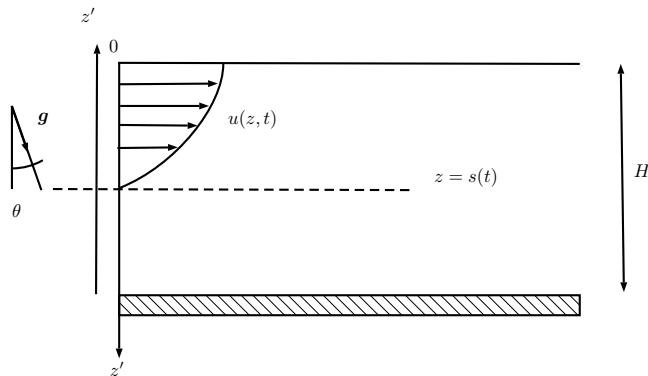


Figure 1: Setting in motion a volume of fluid suddenly tilted at an angle  $\theta$ .

is not bounded by an infinite plate, but by a free surface. As this problem bears some resemblance to the original Stokes problem, this paper refers to it as Stokes' third problem (mainly for convenience). Previously, it was partially studied for viscoplastic flows [2–4].

### 2.1. Governing equations

We consider an incompressible Herschel-Bulkley fluid with density  $\rho$ ; its constitutive equation is discussed in Sec. 2.2. The fluid is initially at rest. There is a free surface located at  $z = 0$ , with the  $z$ -axis normal to the free surface and pointing downward. We also introduce the  $z'$ -axis, normal to the free surface, but pointing upward. The  $x$ -axis is parallel to the free surface. At time  $t = 0$ , the volume is instantaneously tilted at an angle  $\theta$  to the horizontal. We assume that a simple shear-flow takes place under the effects of gravitational forces, and that the flow is invariant under any translation in the  $x$ -direction. The initial velocity is

$$u(z, 0) = 0. \quad (1)$$

At the free surface  $z = 0$ , in the absence of traction, the shear stress  $\tau$  is zero

$$\tau = 0 \text{ at } z = 0. \quad (2)$$

A key issue in this problem is the existence of a propagation front  $z = s(t)$  (i.e. a moving interface between the sheared and stationary layers) and the boundary

conditions at this front. For Stokes' first problem, shear-thinning viscoplastic fluids behave like Newtonian fluids: the momentum balance equation reduces to a linear parabolic equation, and the front propagates downward instantaneously [7, 9]. The question arises as to whether this is also the case for Stokes' third problem.

Let us admit that the interface moves at a finite velocity  $v_f$ . The dynamic boundary condition at this interface is given by a Rankine-Hugoniot equation

$$\llbracket -\rho \mathbf{u}(\mathbf{u} \cdot \mathbf{n} - v_f) + \boldsymbol{\sigma} \cdot \mathbf{n} \rrbracket = 0,$$

where  $\llbracket f \rrbracket$  denotes  $f$ 's jump across the interface [10]. In the absence of slip

$$\mathbf{u} = 0 \text{ at } z = s(t), \quad (3)$$

this equation implies the continuity of the stresses across the interface

$$\llbracket \tau \rrbracket = 0 \text{ and } \llbracket \sigma_{zz} \rrbracket = 0, \quad (4)$$

where  $\sigma_{zz}$  is the normal stress in the  $z$ -direction. If the material slips along the bed-flow interface at a velocity  $u_s$ , then the Rankine-Hugoniot equation implies that the shear stress exhibits a jump across the interface, while the normal stress is continuous

$$\llbracket \tau \rrbracket = -\rho u_s v_f \text{ and } \llbracket \sigma_{zz} \rrbracket = 0.$$

The first relationship has often been used in the form  $v_f = -\llbracket \tau \rrbracket / (\rho u_s)$ , which fixes the entrainment rate when the other variables are prescribed [3, 11, 12]. Internal slip in viscoplastic materials is only partially understood. It may be a consequence of shear localisation or shear banding in thixotropic viscoplastic fluids [13, 14]. In the rest of the paper, we assume that the no-slip condition applies at the interface, and so the boundary condition is given by equation (4).

For this problem, the governing equation is derived from the momentum balance equation in the  $x$ -direction

$$\rho \frac{\partial u}{\partial t} = \rho g \sin \theta - \frac{\partial \tau}{\partial z}. \quad (5)$$

To solve the initial boundary value problem (2)–(5), we need to specify the constitutive equation.

## 2.2. Constitutive equation

For simple shear-flows, the Herschel-Bulkley constitutive equation reads

$$\begin{cases} \dot{\gamma} = 0 & \text{if } \tau < \tau_c, \\ \tau = \tau_c + \kappa|\dot{\gamma}|^n & \text{if } \tau \geq \tau_c, \end{cases} \quad (6)$$

where  $\tau_c$  denotes the yield stress,  $\dot{\gamma} = du/dz$  the shear rate,  $n$  the shear-thinning index (as in most cases  $n \leq 1$ ) and  $\kappa$  the consistency. This equation essentially relies on a phenomenological basis. A tensorial equation can be derived by using a von Mises yield criterion to define the yield surface (i.e. the surface separating sheared from unsheared regions) [1]. The interpretation of Eq. (6) is classic: for the material to flow, the shear stress  $\tau$  must exceed a threshold  $\tau_c$ , called the yield stress. When  $\tau < \tau_c$ , the material remains unsheared.

The existence of a true yield stress was long debated. It is now well accepted that for a class of fluids referred to as *simple yield-stress fluids*, Eq. (6) closely describes the rheological behaviour in steady-state simple-shear flows [15, 16], and in a tensorial form, the Herschel-Bulkley equation offers a correct approximation of three-dimensional flows, notably with regards to the von Mises criterion for yielding [17]. This means that for these fluids in steady state viscometric flows, the shear rate tends continuously to zero when the shear stress approaches the yield stress. For non-simple yield stress fluids, e.g. those exhibiting thixotropy, the shear rate cannot be given a value when  $\tau \rightarrow \tau_c$ : indeed, there may be no homogeneous steady-state flow when the shear rate drops below a finite critical value  $\dot{\gamma}_c$  [15–20]. This also entails that the material exhibits a static yield stress  $\tau_0 > \tau_c$  that differs from the dynamic yield stress  $\tau_c$  in Eq. (6). The steady state constitutive equation reads

$$\tau = \tau_c + \kappa|\dot{\gamma}|^n \text{ if } |\dot{\gamma}| \geq \dot{\gamma}_c, \quad (7)$$

with  $\tau_0 = \tau_c + \kappa\dot{\gamma}_c^n$ . For  $0 < |\dot{\gamma}| \leq \dot{\gamma}_c$ , the rheological behaviour exhibits complex properties (time dependency, a thixotropy loop, shear banding, aging and shear rejuvenation, or minimum in the flow curve ) depending on the material [14–16]. Various approaches have been proposed to incorporate the effect of shear

history in the constitutive equation, but a general framework of the underlying mechanisms is still lacking [14, 18, 21, 22]. For the sake of simplicity, we assume that as the shear rate increases from zero, the shear stress must exceed  $\tau_0$  for a steady state flow to occur. When the shear rate decreases from a sufficiently high value in a steady-state regime, the shear stress follows the flow curve (6) continuously even for  $|\dot{\gamma}| < \dot{\gamma}_c$  [19, 23–25]. Thus, flow cessation and fluidisation cannot be described by a one-to-one constitutive equation.

Prior to yielding, a Herschel-Bulkley material is often considered to behave like an elastic solid. A simple idea is then to supplement the constitutive equation (6) with an equation reflecting the elastic behaviour for  $\tau < \tau_c$ , but this leads to inconsistencies such as the non-uniqueness of the yield function due to finite deformations (and thus normal stresses) in the solid material [26]. One alternative is to use an elastoviscoplastic constitutive equation [27], which extends Oldroyd’s viscoelastic model to plastic materials [28]. Although the model is consistent from a continuum mechanics’ point of view and experimentally [29], it involves nontrivial differential operators (Gordon-Schowalter derivatives), which make analytical calculations intricate. Here, we follow Lacaze et al. [30], who suggested neglecting the nonlinear differential terms in order to end up with an approximate constitutive equation for simple shear flows

$$\frac{1}{G} \frac{\partial \tau}{\partial t} = \dot{\gamma} - \max \left( 0, \frac{|\tau| - \tau_c}{\kappa |\tau|^n} \right)^{1/n} \tau, \quad (8)$$

where  $G$  is the elastic modulus. Under steady state conditions, this equation leads to the Herschel-Bulkley model (6).

### 3. Solution to Stokes’ third problem for simple Herschel-Bulkley fluids

#### 3.1. Dimensionless governing equations

We introduce the following scaled variables

$$u \rightarrow U_* \hat{u}, z \rightarrow H_* \hat{z}, t \rightarrow T_* \hat{t}, \text{ and } \tau \rightarrow \frac{\mu U_*}{H_*} \hat{\tau} \quad (9)$$

with  $U_* = \rho g H^2 \sin \theta / \mu$  the velocity scale,  $H_* = H$  the length scale,  $T_* = H_* / U_*$  the time scale,  $\mu = \kappa(U_*/H_*)^{n-1}$  the bulk viscosity. We also introduce the Reynolds, Bingham and Deborah dimensionless numbers

$$\text{Re} = \frac{\rho U_* H_*}{\mu}, \text{Bi} = \frac{\tau_c}{\mu \frac{U_*}{H_*}}, \text{ and } \text{De} = \frac{\mu U_*}{G H_*}. \quad (10)$$

The governing equations reduce to a nonhomogeneous linear hyperbolic problem

$$\text{Re} \frac{\partial \hat{u}}{\partial \hat{t}} = 1 + \frac{\partial \hat{\tau}}{\partial \hat{z}'}, \quad (11)$$

$$\text{De} \frac{\partial \hat{\tau}}{\partial \hat{t}} = \frac{\partial \hat{u}}{\partial \hat{z}'} - F(\hat{\tau}), \quad (12)$$

with  $F(\hat{\tau}) = \max(0, |\hat{\tau}| - \text{Bi})^{1/n} \hat{\tau} / |\hat{\tau}|$ . The boundary and initial conditions are  $\hat{u} = 0$  at  $\hat{z}' = 0$ ,  $\hat{\tau} = 0$  at  $\hat{z}' = 1$ , and  $\hat{\tau} = \hat{u} = 0$  at  $\hat{t} = 0$ . The analysis of the associated characteristic problem shows that the material starts moving at its base instantaneously when the initial thickness  $H$  is sufficiently large, i.e. for  $\text{Bi} < 1$  (see Appendix A). The disturbance propagates toward the free surface at velocity  $\hat{c} = 1/\sqrt{\text{ReDe}}$ . The time of setting in motion is defined here as the time

$$\hat{t}_c = 1/\hat{c} = \sqrt{\text{ReDe}} \quad (13)$$

needed for this disturbance to reach the free surface.

### 3.2. Numerical solutions

Numerical solutions to the problem (11)–(12) can be obtained using the method of characteristics (see Appendix A). Figure 2 shows an example of the evolution of the velocity profile for a particular set of values of  $\text{De}$ ,  $\text{Re}$ ,  $\text{Bi}$ , and  $n$ . In short time periods ( $\hat{t} < \hat{t}_c$ ), the velocity varies linearly close to the bottom, while the upper layers of the material remain unsheared. For  $\hat{t} \sim \hat{t}_c$ , there is a phase of elastic adjustment, and then at longer time periods ( $\hat{t} > \hat{t}_c$ ), the velocity approaches its steady-state profile characterised by a shear region for  $\hat{z}' \leq \text{Bi}$  and a plug flow for  $\hat{z}' > \text{Bi}$ .

Figure 3 shows the stress evolution. At short time periods ( $\hat{t} < \hat{t}_c$ ), the shear stress varies linearly near the bottom and is zero in the upper layers. The elastic

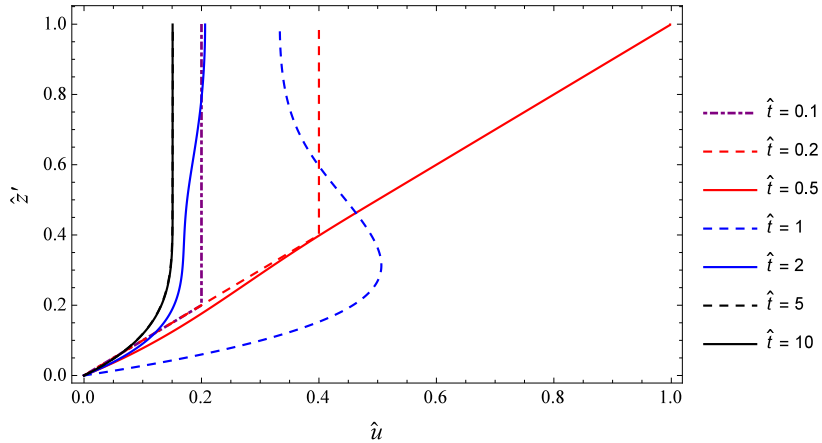


Figure 2: Evolution of the velocity profile for  $De = 0.1$ ,  $Re = 10$ ,  $Bi = 0.5$ , and  $n = 1/3$ . We report the computed velocity profiles at times  $\hat{t} = 0.1, 0.2, 0.5, 1, 2, 5$  and  $10$ . Numerical simulation with  $N = 1,000$  nodes. Here the fluid is set in motion at  $\hat{t}_c = 1$ .

adjustment phase entails the propagation of shear waves that dampen quickly. At long time periods ( $\hat{t} > \hat{t}_c$ ), the shear stress is close to its steady state profile  $\hat{\tau} = 1 - \hat{z}'$ .

#### 4. Solution to Stokes' third problem for non-simple Herschel-Bulkley fluids

When the fluid exhibits a static yield stress  $\tau_0$  that is larger than its dynamic yield stress  $\tau_c$ , it is sufficiently rigid to stand the sudden tilting without deforming instantaneously as long as  $\tau_0 > \rho g H \sin \theta$ . Yet, in such a case, if the free surface becomes sufficiently destabilised (see below), a front propagates downwards from the free surface. This is the result of the fluid destructure during yielding. For the sake of simplicity, we focus on a Bingham fluid ( $n = 1$ ), the results of which can be readily extended to Herschel-Bulkley fluids. We consider a thixotropic Bingham fluid, whose constitutive equation depends on its

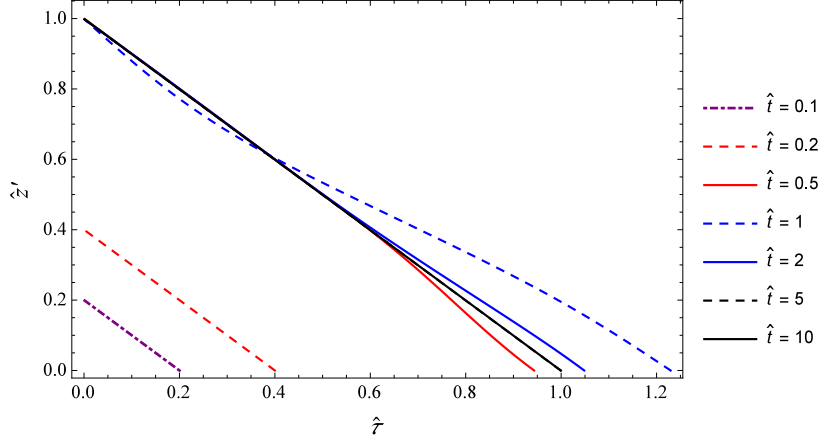


Figure 3: Evolution of the shear stress profile for  $De = 0.1$ ,  $Re = 10$ ,  $Bi = 0.5$  and  $n = 1/3$ . We report the computed velocity profiles at times  $\hat{t} = 0.1, 0.2, 0.5, 1, 2, 5$  and  $10$ .

shear history as follows (see Sec. 2.2 and Fig. 4)

$$\begin{cases} \dot{\gamma} = 0 & \text{if } \tau < \tau_c, \\ \tau = \tau_c + \kappa|\dot{\gamma}| & \text{if } \tau \geq \tau_0 \text{ for increasing } \dot{\gamma}, \\ \tau = \tau_c + \kappa|\dot{\gamma}| & \text{if } \tau \geq \tau_c \text{ for decreasing } \dot{\gamma}. \end{cases} \quad (14)$$

In Stokes' third problem, when the layer is suddenly tilted, the shear stress adopts a linear profile in the absence of motion:  $\tau(z) = \rho g z \sin \theta$ . If this layer is not disturbed, it will stay indefinitely at rest. Contrary to the previous section, we need to alter the initial condition to create motion. Any disturbance in the upper layer  $0 \leq z \leq h_c = \tau_c / (\rho g \sin \theta)$  is quickly dampened, and so we need to disturb the layer in the intermediate region  $h_c \leq z \leq h_0 = \tau_0 / (\rho g \sin \theta)$ . We can also apply a shear stress  $\tau_c$  at the free surface so that the stress state in the upper layer just exceeds the yield stress. For the sake of simplicity, instead of addressing these two scenarios, in the calculations below and without a loss of generality, we assume that the yield stress  $\tau_c$  is zero. We can then return to the original problem by considering that either a sufficient shear stress is applied at the free surface or that the domain of integration lies in the  $h_0 - h_c$  range.

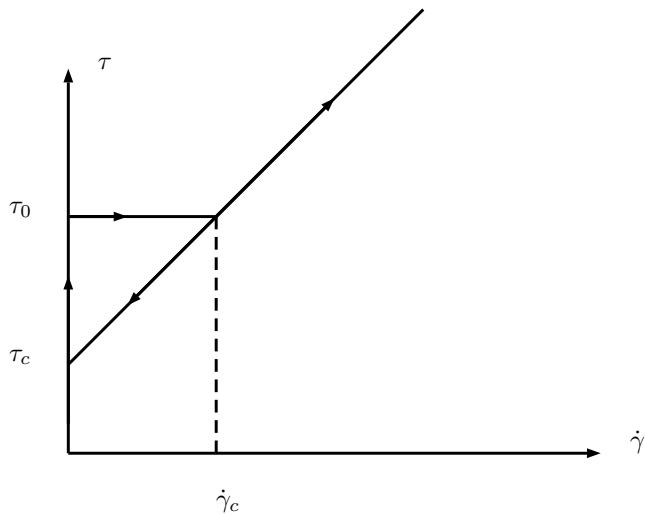


Figure 4: Flow curve. We assume that when the material is at rest, it behaves like a rigid body. When the shear stress exceeds a threshold called the static yield stress  $\tau_0$ , it starts moving, but until the shear rate exceeds a critical shear-rate  $\dot{\gamma}_c$ , there is no steady state. When the shear rate is increased above this critical value, the material behaves like a Bingham fluid. If the shear rate is decreased from a value  $\dot{\gamma} > \dot{\gamma}_c$ , then the shear stress follows another path marked by the down arrow. In that case, it can approach the zero limit continuously, while the shear stress comes closer to the static yield stress  $\tau_c$ .

#### 4.1. Dimensionless governing equations

We make the problem dimensionless using the same scales as in Sec 3. The dimensionless initial boundary value problem is

$$\text{Re} \frac{\partial \hat{u}}{\partial \hat{t}} = 1 + \frac{\partial^2 \hat{u}}{\partial \hat{z}^2}, \quad (15)$$

subject to the boundary conditions at the free surface  $\hat{z} = 0$

$$\frac{\partial \hat{u}}{\partial \hat{z}}(0, \hat{t}) = 0. \quad (16)$$

There is a moving boundary at  $\hat{z} = \hat{s}(\hat{t})$  for which the no-slip condition holds

$$\hat{u}(\hat{s}, \hat{t}) = 0. \quad (17)$$

while the stress continuity (4) across this interface gives

$$\frac{\partial \hat{u}}{\partial \hat{z}}(\hat{s}, \hat{t}) = -\hat{\gamma}_c \text{ with } \hat{\gamma}_c = \hat{\tau}_0 - \text{Bi} > 0. \quad (18)$$

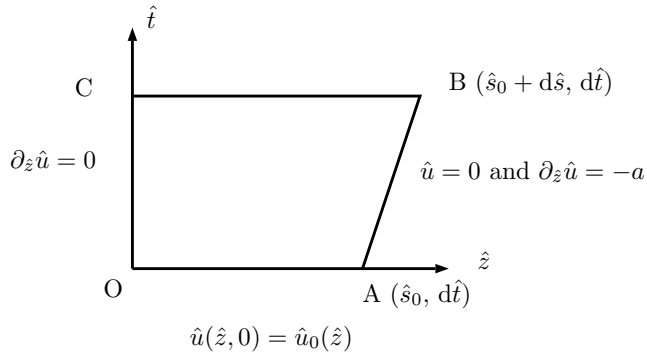


Figure 5: Incipient motion. At time  $t = 0$ , we impose a velocity profile  $\hat{u}_0$  to the layer  $0 \leq \hat{z} \leq \hat{s}_0$ , and so the front is initially at point A. At time  $d\hat{t}$ , the front has reached point B located at  $\hat{s} + d\hat{s}$ .

The initial condition is

$$\hat{u}(\hat{z}, 0) = \hat{u}_0(\hat{z}) \text{ for } 0 \leq \hat{z} \leq \hat{s}_0, \quad (19)$$

with  $\hat{u}_0 > 0$ . For the initial and boundary conditions to be consistent, we also assume that  $\hat{u}'_0(0) = 0$  and  $\hat{u}'_0(\hat{s}_0) = -\hat{\gamma}_c$ .

This initial boundary value problem is very close to the Stefan problem, which describes the evolution in temperature within a medium experiencing a phase transition. As in the Stefan problem, the evolution equation (15) is a linear parabolic equation, but the whole system of equations is nonlinear [31]; this results from the existence of a moving boundary  $\hat{s}(\hat{t})$ , which has to be determined while solving the system (15)–(18). The present problem shows two crucial differences from the Stefan problem: there is a source term in the diffusion equation (15), and the position  $\hat{s}(\hat{t})$  of the moving boundary does not appear explicitly in Eqs. (15)–(18).

#### 4.2. Existence of a solution

Contrary to the Stefan problem, the moving boundary  $\hat{s}(\hat{t})$  will not start moving spontaneously. Part of the fluid must be destabilised prior to incipient motion, and that is the meaning of the initial condition (19). This is also

consistent with the thixotropic behaviour described by the constitutive equation (14).

To show this, let us consider what happens in the earliest moments of motion by using the Green theorem. Initially the interface position is at  $\hat{s}(0) = \hat{s}_0$  (point A in Fig. 5), and after a short time  $\Delta\hat{t}$ , it has moved to  $\hat{s}_0 + d\hat{s}$  (point B in Fig. 5). The displacement increment can be determined by differentiating the boundary condition (17)

$$\frac{d}{d\hat{t}}\hat{u}(\hat{s}, \hat{t}) = \frac{\partial\hat{u}}{\partial\hat{x}}\bigg|_{\hat{s}} \frac{d\hat{s}}{d\hat{t}} + \frac{\partial\hat{u}}{\partial\hat{t}}\bigg|_{\hat{s}} = 0. \quad (20)$$

Using the evolution equation (15) and the boundary condition (18), we deduce

$$\hat{\gamma}_c \frac{d\hat{s}}{d\hat{t}}\bigg|_0 = \frac{1 + u_0''(\hat{s}_0)}{\text{Re}}.$$

We then deduce that the front has moved a distance  $d\hat{s} = (1 + u_0''(\hat{s}_0))d\hat{t}/(\hat{\gamma}_c \text{Re})$ .

Applying the Green theorem to the oriented surface OABC gives

$$\oint_{\text{OABC}} \left( \text{Re} \frac{\partial\hat{u}}{\partial\hat{t}} - \frac{\partial^2\hat{u}}{\partial\hat{z}^2} \right) d\hat{z}d\hat{t} = \int_{\text{OABC}} \text{Re} \hat{u} d\hat{z} + \frac{\partial\hat{u}}{\partial\hat{z}} d\hat{t}.$$

On the path CB, the only condition is that the velocity must be positive:  $\int_{\text{CB}} \hat{u} d\hat{z} > 0$ . Making use of the boundary conditions (16)–(18) and initial condition (19), we find the necessary condition for motion

$$\int_0^{\hat{s}_0} \hat{u}_0 d\hat{z} > \frac{\hat{\gamma}_c + \hat{s}_0}{\text{Re}} d\hat{t} + \frac{1 + u_0''(\hat{s}_0)}{2\hat{\gamma}_c \text{Re}} d\hat{t}^2. \quad (21)$$

No solution satisfies this condition in the limit  $s_0 \rightarrow 0$ . A sufficiently high shear must be applied to the upper layer over a thickness  $\hat{s}_0$  for the flow to start.

#### 4.3. Similarity solution

There is no exact similarity solution to the problem (15)–(18), but we can work out an approximate solution, which describes the flow behaviour in the vicinity of the interface  $\hat{s}(\hat{t})$ . To that end, we seek a solution in the form  $\hat{u}(\hat{z}, \hat{t}) = \hat{t}F(\xi, \hat{t})$  with  $\xi = \hat{z}/\hat{t}$  the similarity variable. Substituting  $\hat{u}$  with this form into the governing equation (15) gives

$$F(\xi, \hat{t}) + \hat{t} \frac{\partial F}{\partial \hat{t}} = \xi \frac{\partial F}{\partial \xi} + 1 + \frac{1}{\hat{t}} \frac{\partial^2 F}{\partial \hat{t}^2}. \quad (22)$$

We then use the expansion  $F(\xi, \hat{t}) = F_0(\xi) + \hat{t}^{\nu_1} F_1(\xi) + \dots + \hat{t}^{\nu_i} F_i(\xi) + \dots$ , with  $F_i$  functions of  $\xi$  alone and  $\nu_i > 0$ . To leading order and in the limit  $\hat{t} \gg 1$ , Eq. (22) can be reduced to a first order differential equation

$$\text{Re}F_0 = 1 + \text{Re}\xi F_0', \quad (23)$$

subject to  $F(\xi_f) = 0$  and  $F'(\xi_f) = -\hat{\gamma}_c$ , where  $\xi_f = \hat{s}/\hat{t}$  is the position of the interface. The solution is

$$F_0 = \frac{1}{\text{Re}} - \hat{\gamma}_c \xi. \quad (24)$$

The solution satisfies the two boundary conditions (17)–(18) at the interface, but not boundary condition (16) at the free surface. A boundary layer correction should be used to account for the influence of this boundary condition. As shown by the numerical solution in Sec. 4.4, the approximate similarity solution (24) offers a fairly good description of the solution, and so we will not go further in this direction.

From this calculation, we deduce that the interface behaves like a travelling wave, whose velocity is constant and fixed by the critical-shear rate:  $\hat{v}_f = (\text{Re}\hat{\gamma}_c)^{-1}$ . The interface position is then

$$\hat{s} = s_0 + \frac{\hat{t}}{\text{Re}\hat{\gamma}_c}. \quad (25)$$

The velocity profile is linear in the vicinity of the interface

$$\hat{u} = \frac{\hat{t}}{\text{Re}} - \hat{z}\hat{\gamma}_c. \quad (26)$$

It can be readily shown that the structure of the travelling wave does not depend on the shear-thinning index  $n$ . Indeed, the details of the constitutive equation affect the structure of the diffusive term in the momentum balance equation, but in the vicinity of the interface, this contribution is negligible compared to the source term. Whatever the value of  $n$ , the critical time period for the interface to travel the distance  $\hat{H} = 1$  is thus

$$\hat{t}_c \sim \text{Re}\hat{\gamma}_c. \quad (27)$$

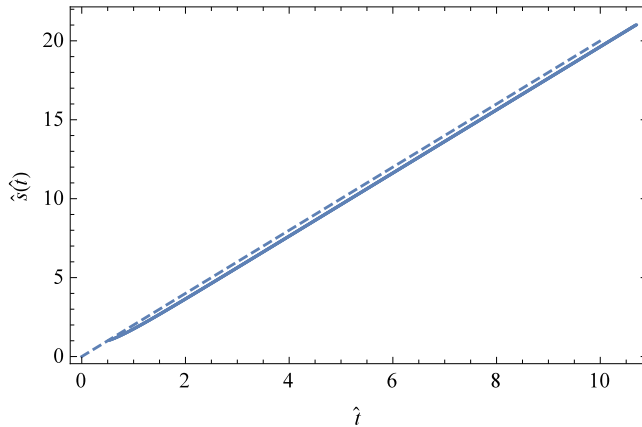


Figure 6: Interface position  $\hat{s}(\hat{t})$  over time. The solid line shows the numerical solution to system (15)–(18) whereas the dashed line represents the approximate solution (25). Numerical solution for  $\hat{\gamma}_c = \hat{\tau}_0 - \text{Bi} = 0.5$  and  $\text{Re} = 1$ .

#### 4.4. Numerical solution

We used a finite-difference scheme to solve the system (15)–(18) (see Appendix B for the details). In Figures 6 to 8, we show an example of a simulation for  $\hat{\gamma}_c = 0.5$ . For the initial disturbance, we assumed that the velocity profile was

$$\hat{u} = \frac{\hat{\gamma}_c}{2} \hat{s}_0 \left( 1 - \left( \frac{\hat{z}}{\hat{s}_0} \right)^2 \right),$$

with  $\hat{s}_0=1$ . The mesh size was  $h = 0.01$ . Figure 6 shows the interface position as a function of time. The analytical solution (25) closely matches the numerical solution, confirming that the disturbance grows and propagates as a travelling wave. Figure 7 shows the velocity profiles at different times. These profiles show that the approximate similarity solution (26) provides a fairly good description of the velocity profile over 75% of the depth. Figure 8 shows the shear stress profiles, which were obtained by numerical integration of the numerical solution. Except for the initial time, the shear stress spans the range  $[0, \hat{\tau}_0 - \text{Bi}]$  (as expected considering the boundary conditions imposed). Over longer time periods, the shear stress is close to the static yield stress  $\tau_0$  over a large part of the depth.

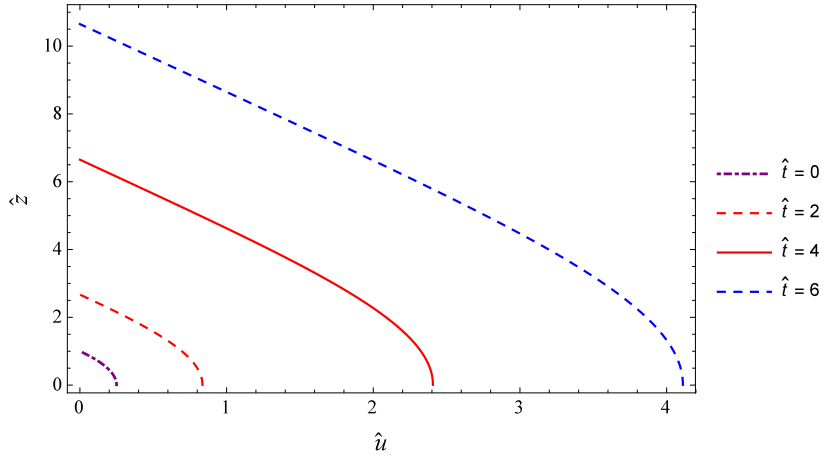


Figure 7: Velocity profiles for  $\hat{t} = 0, 2, 4$  and  $6$ . Numerical solution to Eqs. (15)–(18) for  $\hat{\gamma}_c = \hat{\tau}_0 - \text{Bi} = 0.5$  and  $\text{Re} = 1$ .

## 5. Dam-break wave eroding a stationary layer

This section examines the effects of basal entrainment on the front motion of a viscoplastic avalanche. Let us consider that at time  $t = 0$ , an avalanche made up of a Herschel-Bulkley fluid is released from a reservoir. Initially the fluid material flows over a sloping solid boundary. The bottom inclination is denoted by  $\theta$ . At time  $t = t_0$ , the material encounters a stationary layer made up of the same fluid and occupying a step of length  $\ell_{bed}$  (see Fig. 9). The viscoplastic flow spreads across this stationary layer and entrains part of it. The front position is denoted by  $x_f(t)$ , the flow depth by  $h(x, t)$  and the velocity field by  $\mathbf{u} = (u, w)$ . We use a Cartesian frame with the  $x$ -axis pointing downward and the  $z$ -axis normal to the slope.

To solve this problem, we use lubrication theory. Within the framework of this theory, the momentum balance equations are simplified by neglecting inertia terms and the streamwise gradient of the normal stress. This makes it possible to deduce the pressure and shear stress distributions to the leading order. Making use of the constitutive equation then leads to the velocity profile and, finally, the depth-averaged mass conservation provides the evolution equation for the flow

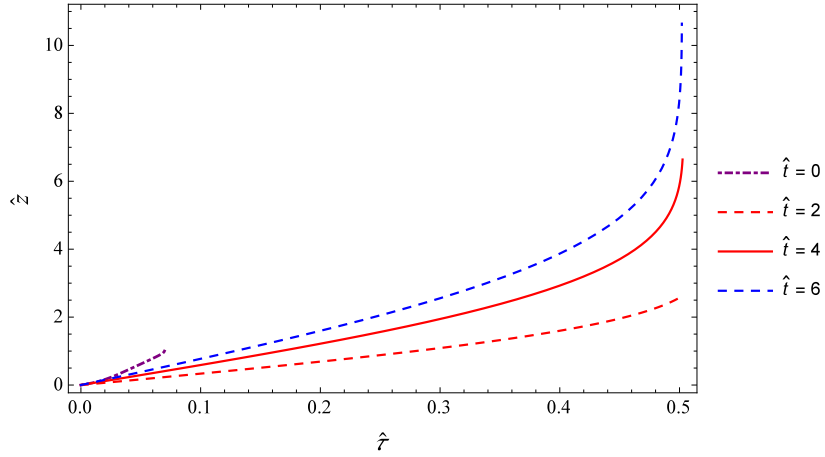


Figure 8: Shear stress profiles for  $\hat{t} = 0, 2, 4$  and  $6$ . Numerical solution to Eqs. (15)–(18) for  $\hat{\gamma}_c = \hat{\tau}_0 - \text{Bi} = 0.5$  and  $\text{Re} = 1$ .

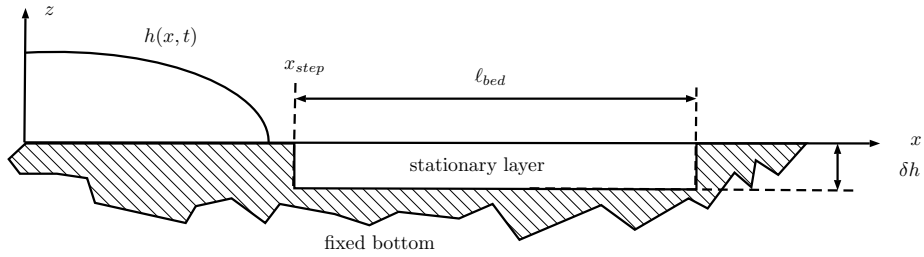


Figure 9: Configuration of the flow. A viscoplastic avalanche is released from a reservoir. It flows over a sloping rigid bed until it gets in contact with a stationary layer made of the same fluid.

depth  $h(x, t)$ . There is a large body of work applying this theory to viscoplastic flows [32–37]; it is succinctly summarised in the next section.

### 5.1. Solution for rigid bottoms

In the limit of low Reynolds number and small aspect ratio numbers, motion is dictated by the balance between the streamwise gradient of the pressure  $\partial_x p$ , gravitational forces and the cross-stream gradient of the shear stress  $\partial_y \tau$ . To the first order, the pressure  $p$  adopts a hydrostatic distribution, while the shear stress  $\tau$  follows a linear distribution whose coefficient is controlled by the bed

slope and free surface gradient:

$$p = \rho g(h - z) \cos \theta \text{ and } \tau = \rho g \sin \theta (h - z) \left( 1 - \cos \theta \frac{\partial h}{\partial x} \right). \quad (28)$$

These expressions hold regardless of the constitutive equation.

We now consider the constitutive equation (6) for simple Herschel-Bulkley materials. These materials flow when the basal-shear stress exceeds the yield stress  $\tau_c$ . When this condition is satisfied, there exists a surface  $z = Y(x, t)$  where the shear stress equals the yield stress:

$$Y = h - \frac{\tau_c}{\rho g \sin \theta \left| 1 - \cot \theta \frac{\partial h}{\partial x} \right|}. \quad (29)$$

Below this surface, the fluid is sheared and above this surface it moves like a plug.

Equations (6) and (28) lead to the following expression for the streamwise velocity component  $u(x, z, t)$

$$u(x, z, t) = \frac{n}{n+1} A \left( 1 - S \frac{\partial h}{\partial x} \right)^{1/n} \left( Y^{1+1/n} - (Y - z)^{1+1/n} \right) \text{ for } 0 \leq z \leq Y, \quad (30)$$

with

$$A = (\rho g \sin \theta / \kappa)^{1/n} \text{ and } S = \cot \theta. \quad (31)$$

For  $z > Y$ , the velocity is constant and equal to the plug velocity  $u_p = u(x, z = Y, t)$ .

Integration of the continuity equation leads to the bulk mass conservation equation

$$\frac{\partial h}{\partial t} + \frac{\partial h \bar{u}}{\partial x} = 0, \quad (32)$$

with  $\bar{u}$  the depth-averaged velocity obtained by integration of the velocity field (30)

$$\bar{u} = \frac{1}{h} \int_0^h u(x, z, t) dz = \frac{A}{h} \frac{n Y^{1+1/n}}{(2n+1)(n+1)} \left( 1 - S \frac{\partial h}{\partial x} \right)^{1/n} (n(h-Y) + (n+1)h). \quad (33)$$

## 5.2. Extension to erodible bottoms

At time  $t = t_0$ , the flow front is about to enter the erodible domain, where a layer of fluid is held initially at rest behind a backwards step (see Fig. 9). The stationary fluid lies between  $z = 0$  and  $z = b(x) \leq 0$ , defining a rigid base below which entrainment is impossible.

The problem of basal entrainment can be greatly simplified by considering that the transmission of stress into the bed occurs very quickly, almost instantaneously, and from the outset, the velocity between the overriding avalanche and the bed is continuous. Indeed, in sections 3 and 4 we determined the characteristic time point  $t_c$  at which a layer of Herschel-Bulkley fluid was set in motion once it has been suddenly tilted. The solution to this problem greatly depends on the details of the constitutive equation. For simple Herschel-Bulkley fluids, the material starts flowing by slipping along its base, provided that  $\text{Bi} < 1$ . Fluidisation occurs from bottom to top during a characteristic time period  $\hat{t}_c = \sqrt{\text{ReDe}}$ . For non-simple Herschel-Bulkley fluids, the material starts to deform where it was disturbed, and the bed-flow interface moves quickly from top to bottom. To illustrate how fast fluidisation occurs, we consider a Herschel-Bulkley fluid with index  $n = 1/3$ , yield stress  $\tau_c = 100$  Pa, consistency  $\kappa = 50$  Pa s <sup>$n$</sup>  and elastic modulus  $G = 100$  Pa; the static yield (if used) is set to  $\tau_0 = 120$  Pa. We consider a 10-cm thick layer tilted at an angle  $\theta = 10^\circ$  to the horizontal. If the fluid is simple, then  $t_c \sim 0.3$  s, whereas for a non-simple fluid, we get  $t_c \sim 9$  ms. Calculation of the characteristic times for Stokes' first problem, studied in [7, 9], led to similar estimates of  $t_c$ . The numerical application thus shows that fluidisation occurs nearly instantaneously in shallow viscoplastic layers.

Equation (32) can be extended to varying bottoms (see Appendix C)

$$\frac{\partial h}{\partial t} + A \frac{\partial}{\partial x} \left( \frac{n(Y-b)^{1+1/n}}{(1+n)(1+2n)} \left( 1 - S \frac{\partial h}{\partial x} \right)^{1/n} (n(h-Y) + (n+1)(h-b)) \right) = 0. \quad (34)$$

### 5.3. Numerical solution

We consider a viscoplastic dam-break wave eroding a layer of viscoplastic fluid of thickness  $\delta h$  and length  $\ell_{bed}$  (see Fig. 9). We solve Eq. (34), which is a nonlinear, parabolic, partial differential equation, for determining the front position  $x_f$  and the flow depth profile  $h(x, t)$ . We used the inbuilt MatLab solver *pdepe* to do this. Note that the Galerkin method [38] used in this solver is unable to cope with shocks. We therefore smoothed the discontinuities in the topography at each end of the step by approximating the step as  $b(x) = -\delta h/2(\tanh(a(x - x_{step})) - \tanh(a(x - x_{step} - \ell_{bed})))$  where  $a$  is a free parameter. In practice, setting  $a = 10^3$  provided good results (for mesh size  $\Delta x = 0.5$  mm, the thickness of the regularised step was 4 mm, i.e.  $8\Delta x$ ). Using no-flux boundary conditions at each end, we solved the governing equation (34) for the flow depth.

Figure 10(a) shows the flow depth evolution for a viscoplastic avalanche released from a reservoir of length  $\ell_{res} = 30$  cm and volume (per unit width)  $V_0 = 0.05$  m<sup>2</sup>, in the absence of entrainment ( $\delta h = 0$ ). Figures 10(a-b) show how basal entrainment alters the flow depth profile. The depth of the stationary layer is either  $\delta h = 1$  cm or  $\delta h = 2$  cm, and its length is the same ( $\ell_{bed} = 20$  cm). When the material flows over the stationary layer, it accelerates, which is reflected by a decrease in the flow depth. The material decelerates as soon as it reaches the fixed bottom. When the front lies over the erodible bed, the flow depth profile is blunter. Figure 10(d) shows the front position with time: the acceleration produced by the stationary layer is clearly visible whereas its deceleration is less marked. The deeper the stationary layer, the more vigorously the front accelerates. Contrary to Newtonian fluids, for which there is little difference between a solution with and without basal entrainment [39], we find that basal entrainment produces a noticeable increase in the front position in the long run.

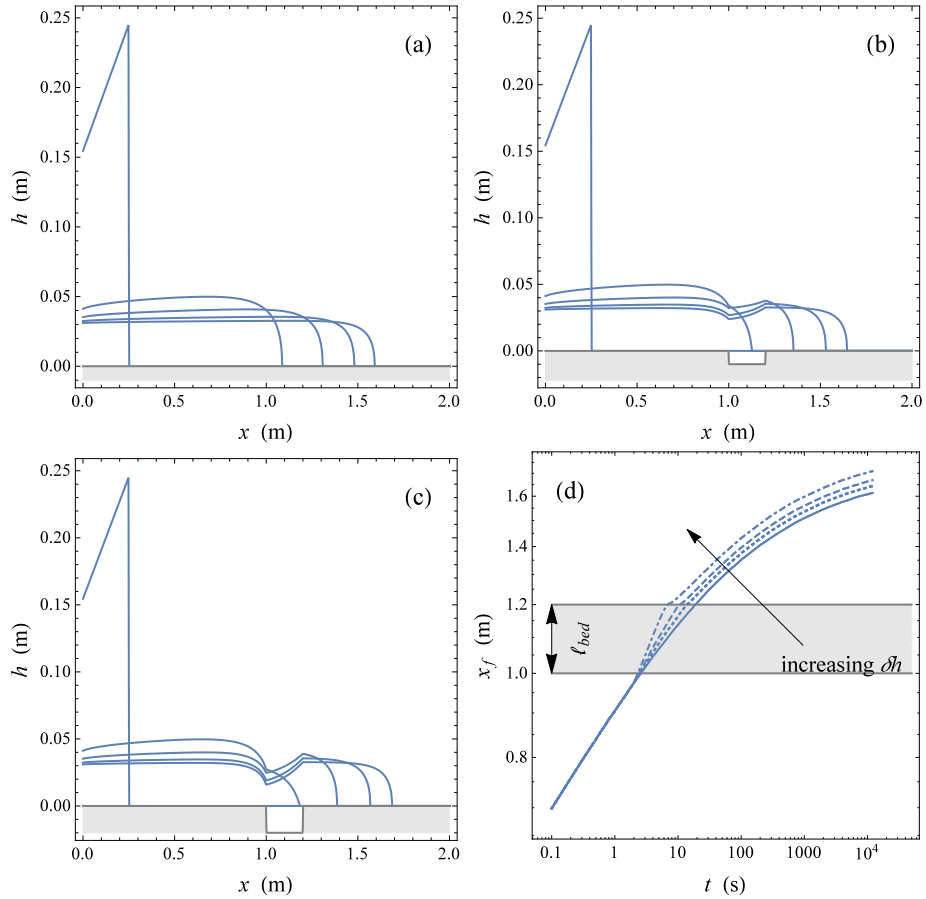


Figure 10: Viscoplastic avalanche over a stationary layer of length  $\ell_{bed} = 20$  cm. (a–c) Flow depth profiles at times  $t = 0, 6$  s, 60 s, 600 s and 6,000 s. (a) Bed depth  $\delta h = 0$  (no entrainment). (b)  $\delta h = 1$  cm. (c)  $\delta h = 2$  cm. (d) Front position with time for different heights  $\delta h$  of the stationary layer: solid line  $\delta h = 0$  (no entrainment), dotted line  $\delta h = 0.5$  cm, dashed line  $\delta h = 1$  cm, dot-dash line  $\delta h = 2$  cm. The grey area indicates the stationary layer. Computations for a Herschel-Bulkley fluid of index  $n = 1/3$ , consistency  $\kappa = 50 \text{ Pa s}^{1/n}$ , yield stress  $\tau_c = 100$  Pa. The initial volume (per unit width) is  $V_0 = 0.05 \text{ m}^2$  and the slope is  $\theta = 30^\circ$ .

## 6. Concluding remarks

In this paper, we investigated Stokes' third problem with the aim of calculating the characteristic time period  $t_c$  for a layer of thickness  $H$  to be set in motion. For simple Herschel-Bulkley fluids, the base of the layer is unable to resist a shear stress and the material starts moving instantaneously. The characteristic time period  $t_c$  is then defined as the time needed for the initial disturbance to propagate from the bed to the free surface. We found that  $\hat{t}_c = \sqrt{\text{ReDe}}$  or dimensionally,  $t_c = H\sqrt{\rho/G}$ . For non-simple Herschel-Bulkley fluids, the material needs to be destabilised. Equation (21) provides a necessary condition for the initial disturbance to create motion. The disturbance propagates down to the bottom at a constant velocity. The time needed to cross the static layer is  $\hat{t}_c = \text{Re}\hat{\gamma}_c$  or dimensionally,  $t_c = H(\tau_0 - \tau_c)/(\mu g \sin \theta)$ . In both cases, this characteristic time period is short.

There is no significant difference between Stokes' first and third problems with regards to a Herschel-Bulkley material's dynamic response when suddenly solicited. One important result of this study was to shed light on the role played by the dynamic yield stress in this time-dependent problem. When the dynamic and static yield stresses coincide and the fluid behaves like a viscoelastoplastic material, the governing equations are linear and hyperbolic. There is no moving boundary separating sheared and unsheared regions. The situation does not differ from that found for Stokes' first problem [7, 9] except that in the present case, even shear-thickening fluids ( $n > 1$ ) do not produce moving boundaries. When the dynamic yield stress exceeds the static yield stress and the fluid behaves like a rigid body in the static regime, the governing equations are nonlinear and parabolic. There is a moving boundary that separates the static and flowing layers. We conclude that Herschel-Bulkley materials are set in motion quickly and this can be assumed to be instantaneous if the flow timescale is much longer than  $t_c$ .

Stokes' third problem has been addressed by a few authors in recent years. Eglit and Yakubenko [2] solved the problem for a non-simple Bingham fluid

numerically. They regularised the constitutive equation by using a biviscous fluid. They observed that the interface moved as a travelling wave with velocity  $v_f = \mu g \sin \theta / (\tau_0 - \tau_c)$ , as we did, but their numerical simulations were not in full agreement with our results: they found that the thickness of the plug region grew indefinitely and that the interface velocity depended on consistency when the fluid was shear thinning. Our analysis considers that the thickness of the plug region is bounded by  $h_c = \tau_c / (\rho g \sin \theta)$ . We found that locally, the interface behaved like a travelling wave whose velocity depended only on the difference  $\Delta\tau = \tau_0 - \tau_c$  regardless of  $n$ . As Eglit and Yakubenko [2] did not give much detail to their numerical solution, it is difficult to appreciate the reasons for this disagreement. Issler [3] investigated Stokes' third problem for non-simple Herschel-Bulkley fluids, but to remove time dependence, he assumed that the mobilised material was of constant thickness. By assuming the existence of a travelling wave solution, he ended up with an expression of the interface velocity  $v_f$ , but due to his working assumption, there is no agreement between his solution and our calculations. Bouchut et al. [4] also studied Stokes' third problem, but for plastic materials with a Drucker-Prager yield criterion (i.e. with a yield surface that depends on the first invariant of the stress tensor). They worked out an exact solution for purely plastic materials (i.e. with zero viscosity) that showed that motion dies out quickly after an initial disturbance.

To the best of our knowledge, there is no experimental data with which compare the theoretical predictions for Stokes' third problem. In a companion paper, we tested the shallow-flow model (34) and found excellent agreement with regards to the front position  $x_f(t)$ . The characteristic time period associated with the solid to fluid transition was investigated in Couette cells. For simple yield stress fluids, careful rheometric investigations have revealed that the transition from solid-like to fluid-like behaviour does not occur instantaneously, but over a length of time  $t_f$  that scales as  $t_f \propto (\tau - \tau_c)^{-p}$  with  $p$  in the 3–8 range under controlled stress experiments [40] or  $t_f \propto \dot{\gamma}^{-q}$  with  $q$  in the 1.8–3.1 range under controlled shear-rate experiments [41], with  $n = q/p$ . Nor does this fluidisation process occur homogeneously throughout the sample, rather it involves

several local processes such as creep, elastic recoil, wall slip and shear banding [42, 43]. From this perspective, it is not certain that the steady-state constitutive equations (6) and (7) are sufficient to capture the dynamics of yielding in Stokes problems.

### Acknowledgements

The work presented here was supported by the Swiss National Science Foundation under Grant No. 200021\_146271/1, a project called ‘‘Physics of Basal Entrainment.’’ The authors are grateful to two anonymous reviewers for their feedback and to Anne Mangeney for discussions. The scripts used for computing Figures 2 to 3, 6 to 8, 10, and B.13 are available from the *figshare* data repository: [dx.doi.org/10.6084/m9.figshare.3496754.v1](https://dx.doi.org/10.6084/m9.figshare.3496754.v1).

### Appendix A. Characteristic problem

In this appendix, we show how the problem (11)–(12) can be cast in characteristic form and how this can be used to solve the problem numerically.

The initial boundary value problem (11)–(12) addressed in Section 3 can be cast in matrix form

$$\frac{\partial}{\partial t} \mathbf{X} + \mathbf{A} \cdot \frac{\partial}{\partial z'} \mathbf{X} = \mathbf{B} \quad (\text{A.1})$$

subject to  $u = 0$  at  $z' = 0$ ,  $\tau = 0$  at  $z' = 1$ , and  $\tau = u = 0$  at  $t = 0$ . The hat annotation has been removed for the sake of simplicity. We have introduced

$$\mathbf{X} = \begin{pmatrix} u \\ \tau \end{pmatrix}, \mathbf{A} = - \begin{pmatrix} 0 & \text{Re}^{-1} \\ \text{De}^{-1} & 0 \end{pmatrix}, \text{ and } \mathbf{B} = \begin{pmatrix} \text{Re}^{-1} \\ -\text{De}^{-1} F(\tau) \end{pmatrix}. \quad (\text{A.2})$$

We now introduce the Riemann variables  $r = -\eta u + \tau$  and  $s = \eta u + \tau$ , where  $\eta = \sqrt{\text{Re}/\text{De}}$ . The eigenvalues of  $\mathbf{A}$  are constant and of opposite sign:  $\pm\lambda$  with  $\lambda = 1/\sqrt{\text{ReDe}}$ , which means that the characteristic curves are straight lines (see Fig. A.11):  $z' = \pm\lambda t + c$  (with  $c$  a constant). The characteristic form of (A.1)

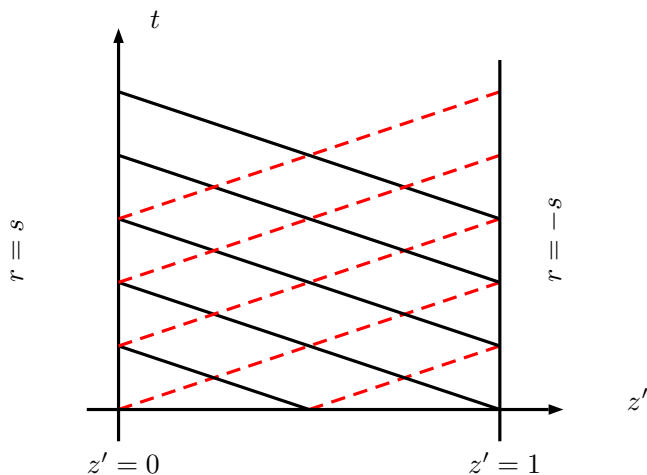


Figure A.11: Characteristic diagram showing the two families of characteristic curves.

is

$$\frac{dr}{dt} = R(\tau) = -\lambda - De^{-1}F(\tau) \text{ along } \frac{dz'}{dt} = \lambda, \quad (\text{A.3})$$

$$\frac{ds}{dt} = S(\tau) = \lambda - De^{-1}F(\tau) \text{ along } \frac{dz'}{dt} = -\lambda, \quad (\text{A.4})$$

with the boundary conditions  $r = s$  at  $z' = 0$  and  $r = -s$  at  $z' = 1$ . The initial conditions are  $r = s = 0$  at  $t = 0$ . As the source term is nonlinear in  $\tau$ , this system of equations has no analytical solution, but it lends itself more readily to numerical solutions.

The domain is divided into  $N - 1$  intervals whose nodes are  $z_i = i\delta x$ , with  $\delta z = 1/N$ , for  $0 \leq i \leq N$ . The center of each interval is  $z_{i+1/2} = (z_i + z_{i+1})/2$ . The numerical integration of the system (A.3)–(A.4) involves two steps. We assume that we know the values  $r_i^{2k}$  and  $s_i^{2k}$  of  $r$  and  $s$  at each node at time  $t = 2k\delta t$  with  $\delta t = \delta x/2/\lambda$ . At time  $t + \delta t$ , a first-order discretisation of (A.3)–(A.4) is

$$r_{i+1/2}^{2k+1} = r_i^{2k} + R(\tau_i^{2k})\delta t \text{ and } s_{i+1/2}^{2k+1} = s_{i+1}^{2k} + S(\tau_{i+1}^{2k})\delta t, \quad (\text{A.5})$$

for  $0 \leq i \leq N - 1$ . At time  $t + 2\delta t$ , we have

$$r_i^{2k+2} = r_{i-1/2}^{2k+1} + R(\tau_{i-1/2}^{2k+1})\delta t \text{ and } s_i^{2k+2} = s_{i+1/2}^{2k+1} + S(\tau_{i+1/2}^{2k+1})\delta t, \quad (\text{A.6})$$

for  $1 \leq i \leq N - 1$ , while at the boundaries, we have

$$r_0^{2k+2} = s_0^{2k+2} \text{ and } s_0^{2k+2} = s_{1/2}^{2k+1} + S(\tau_{1/2}^{2k+1})\delta t, \quad (\text{A.7})$$

and

$$r_N^{2k+2} = r_{N-1/2}^{2k+1} + R(\tau_{N-1/2}^{2k+1})\delta t \text{ and } s_N^{2k+2} = -r_N^{2k+2}. \quad (\text{A.8})$$

At each time step, the velocity and shear stress are thus

$$\tau_i^j = \frac{1}{2}(r_i^j + s_i^j) \text{ and } u_i^j = \frac{1}{2\eta}(s_i^j - r_i^j). \quad (\text{A.9})$$

## Appendix B. Numerical solution to the Stefan-like problem

In this appendix, we propose a finite-difference algorithm for the Stefan-like problem (15). Various techniques have been developed to solve Stefan problems [31, 44–47]. Here we take inspiration from Morland [48]. By modifying one of the boundary conditions, we can work out a similarity solution which is then used to test the algorithm accuracy.

### Appendix B.1. Numerical scheme

For the sake of brevity, we omit the hat annotation in this appendix. We make the following change of variable

$$u(z, t) = \tilde{u}(z, s),$$

where time has been replaced by  $s$ . Assuming that  $s(t)$  is a continuous monotonic function of time and  $\dot{s}(t) > 0$ , the Jacobian of the transformation is non-zero. The advantage of this change of variable is that the front position appears explicitly in the governing equations and the domain of integration now has known boundaries. We must solve the following initial boundary value problem

$$\text{Re}\alpha(s)\frac{\partial\tilde{u}}{\partial s} = 1 + \frac{\partial^2\tilde{u}}{\partial z^2} \text{ with } \alpha(s) = \frac{ds}{dt} \quad (\text{B.1})$$

subject to the boundary conditions at the free surface

$$\frac{\partial\tilde{u}}{\partial z}(0, s) = 0. \quad (\text{B.2})$$

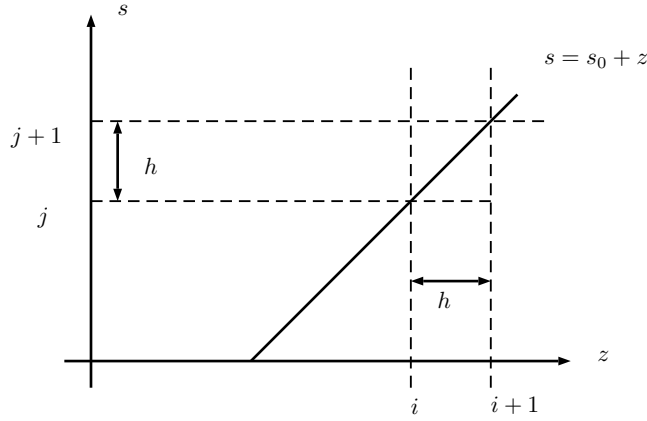


Figure B.12: Domain of integration. The change of variable  $t \rightarrow s$  makes it possible to work on a fixed domain, where the upper bound  $s$  is fixed in advance:  $s = s_0 + z$ .

There is a moving boundary at  $z = s(t)$  for which the no-slip condition holds

$$\tilde{u}(s, s) = 0. \quad (\text{B.3})$$

while the stress continuity (4) across this interface gives

$$\frac{\partial \tilde{u}}{\partial z}(s, s) = -\dot{\gamma}_c \text{ with } \dot{\gamma}_c = \tau_0 - \text{Bi} > 0. \quad (\text{B.4})$$

The initial condition is

$$\tilde{u}(z, s_0) = \tilde{u}_0(z) \text{ for } 0 \leq z \leq s_0. \quad (\text{B.5})$$

Once the solution  $\tilde{u}(x, s)$  has been calculated, we can return to the original variables by integrating  $\alpha(s)$

$$t = \int_{s_0}^s \frac{ds'}{\alpha(s')}. \quad (\text{B.6})$$

The numerical strategy is the following. The domain of integration is discretised using a uniform rectangular grid with a fixed mesh size  $h$ . Time  $t$ , and thus parameter  $\alpha$ , are calculated at each iteration so that the front has moved a distance  $h$  (see Fig. B.12). The value of the numerical solution at  $z = ih$  and  $s = jh$  is denoted by  $u_i^j$ . The front position at time step  $jh$  is denoted

by  $s^j = s_0 + jh$ . We use an implicit finite-difference scheme for discretising the spatial derivatives and an explicit forward Euler for the time derivative in Eq. (B.1):

$$-ru_{i-1}^{j+1} + (2r + a^{j+1})u_i^{j+1} - ru_{i+1}^{j+1} = h^2 + (1-r)u_{i-1}^j + (a^j - 2r)u_i^j + (1-r)u_{i+1}^j,$$

where  $0 < r \leq 1$  is a weighting coefficient and  $a^j = \text{Re } h\alpha^j$ , for  $2 \leq i \leq j$ . In practice, we take  $r = 1/2$  (Crank-Nicolson scheme). The boundary condition (B.2) is discretised as follows

$$ru_2^{j+1} - ru_1^{j+1} = (1-r)u_1^j + (1-r)u_2^j, \quad (\text{B.7})$$

While the boundary condition (B.4) gives

$$ru_{j+1}^{j+1} - ru_{j-1}^{j+1} = (1-r)u_{j-1}^j + (1-r)u_{j+1}^j - 2h\dot{\gamma}_c. \quad (\text{B.8})$$

The scheme involves the value  $u_{j+1}^j$  outside the domain of integration. We use a second-order Taylor-series extrapolation

$$u_{j+1}^j = -\dot{\gamma}_c h - \frac{1}{2}h^2(1 - \text{Re } \alpha^j \dot{\gamma}_c), \quad (\text{B.9})$$

where we use the boundary condition (B.3)  $u_j^j = 0$ , the boundary condition (B.3) for the first-order term, and Eqs. (17) and (B.1) for the second-order term.

At time step  $j + 1$ , we thus have to solve the system of  $j + 1$  equations

$$\mathbf{P}(r, h, \alpha^{j+1}) \cdot \mathbf{U}^{j+1} = \mathbf{Q}(r, h, \alpha^{j+1}) \cdot \mathbf{U}^{j+1} + \mathbf{R}(h, \dot{\gamma}_c),$$

where  $\mathbf{P}$  and  $\mathbf{Q}$  are tridiagonal matrices and  $\mathbf{R}$  is a constant vector, whose entries are given by Eqs. (B.7)-(B.9). The coefficient  $\alpha^{j+1}$  is adjusted until the boundary condition (B.3) is satisfied:  $u_{j+1}^{j+1} = 0$ . To that end, we use the secant method:

$$s^{j+1,(k+1)} = s^{j+1,(k)} - \frac{s^{j+1,(k)} - s^{j+1,(k-1)}}{u_{j+1}^{j+1,(k)}(s^{j+1,(k)}) - u_{j+1}^{j+1,(k-1)}(s^{j+1,(k-1)})}$$

where  $s^{j+1,(k+1)}$  the  $k$ th iteration to find  $s^{j+1}$ . The stopping criterion is

$$\left| s^{j+1,(k+1)} - s^{j+1,(k)} \right| < h^2 \left| s^{j+1,(k)} \right|.$$

Usually, only a few iterations are required to find  $\alpha^{j+1}$ . To estimate time  $t$ , we integrate Eq. (B.6) numerically by approximating the integrand using a second-order polynomial. We can then iteratively calculate  $t^j$

$$t^{j+1} = t^{j-1} + \frac{h}{3} \left( \frac{1}{\alpha^{j+1}} + \frac{4}{\alpha^j} + \frac{1}{\alpha^{j-1}} \right).$$

### *Appendix B.2. Testing the algorithm*

The initial boundary value problem (B.1)–(B.4) has no similarity solution, but if we replace the boundary (B.4) with

$$\frac{\partial \tilde{u}}{\partial z}(s, s) = -as, \quad (\text{B.10})$$

where  $0 < a < 1$  is a free parameter, then we can work out a similarity solution

$$u(x, t) = tU(\eta) \text{ with } \eta = \frac{x}{b\sqrt{t}}, b = \sqrt{2\frac{1-a}{a}}, \quad (\text{B.11})$$

and

$$U(\eta) = \frac{b^2}{2+b^2}(1-\eta^2).$$

The front position is given by

$$s(t) = s_0 + b\sqrt{t}. \quad (\text{B.12})$$

The algorithm of Appendix B.1 was adapted to take the change in the boundary condition into account. Figure B.13 shows a comparison between the numerical solution and the analytical solution (B.12). The initial condition is the solution (B.10) reached by  $u$  at time  $t_0 = (s_0/b)^2$ . The initial front position is arbitrarily set to  $s_0 = 50h$ . There is a fairly good agreement, but even if the algorithm is a second order one, errors accumulate. In the example in Figure B.13, the error reaches 1.8% after 10,000 iterations.

## **Appendix C. Derivation of the extended evolution equation**

In this appendix, we derive the evolution equation (34).

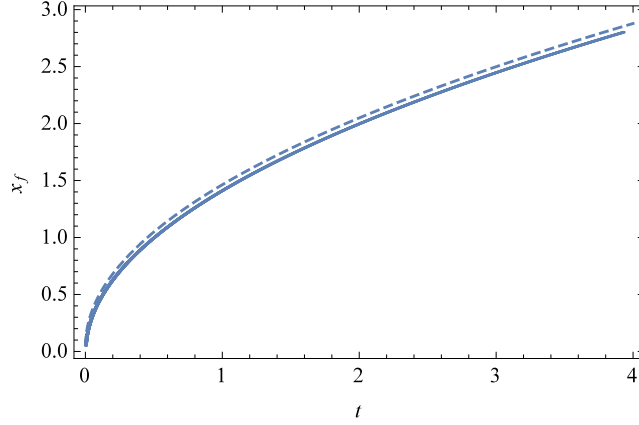


Figure B.13: Comparison of the numerical solution (solid line) and the analytical solution (dashed line) given by Eq. B.12. Simulation for  $a = 0.5$  and  $h = 10^{-3}$ .

In the shear-layer velocities will have the subscript  $S$ , and in the plug layer they will have the subscript  $P$ . Applying the no-slip boundary condition  $u_S(x, z = b(x), t) = 0$  on the rigid surface  $b(x)$  and solving

$$\left| \frac{\partial u}{\partial z} \right| = \left( \frac{1}{K} \left( \rho g \sin \theta (h - z) \left( 1 - \cot \theta \frac{\partial h}{\partial x} \right) - \tau_c \right) \right)^{1/n}. \quad (\text{C.1})$$

gives an equation for the velocity below the yield surface, in the shear layer:

$$u_S(x, z, t) = \frac{nA}{n+1} \left( 1 - S \frac{\partial h}{\partial x} \right)^{1/n} \left( (Y(x, t) - b(x))^{1/n} - (Y(x, t) - z)^{1+1/n} \right). \quad (\text{C.2})$$

In this arbitrary geometry the yield surface is now

$$Y(x, t) = \max \left( h - \frac{\tau_c}{\rho g \left| 1 - S \frac{\partial h}{\partial x} \right|}, b(x) \right). \quad (\text{C.3})$$

Then, in the plug layer,

$$u_P(x, t) = \frac{n}{n+1} A \left( 1 - S \frac{\partial h}{\partial x} \right)^{1/n} \left( (Y(x, t) - b(x))^{1+1/n} \right). \quad (\text{C.4})$$

The mass conservation equation is then used to obtain expressions for  $\partial w_S / \partial z$  and  $\partial w_P / \partial z$ . These can be integrated using the no-slip condition  $\mathbf{u}_S \cdot \mathbf{n} = 0$

fixing the constant of integration below the yield surface, and the continuity of the velocity across the yield surface fixing the constant in the pseudo-plug region. Thus:

$$\begin{aligned}
w_S(x, z, t) &= \frac{S \frac{\partial^2 h}{\partial x^2}}{n+1} \left(1 - S \frac{\partial h}{\partial x}\right)^{1/n-1} A \left( \frac{n}{2n+1} \left( (Y-z)^{\frac{2n+1}{n}} - (Y-b)^{2+1/n} \right) \right. \\
&+ (Y-b)^{1+1/n}(z-b) \\
&- \left. \left(1 - S \frac{\partial h}{\partial x}\right)^{1/n} A \left( \left( \frac{\partial Y}{\partial x} - \frac{\partial b}{\partial x} \right) (Y-b)^{1/n}(z-b) \right) \right. \\
&+ \left. \frac{n \frac{\partial Y}{\partial x}}{n+1} \left( (Y-z)^{1+1/n} - (Y-b)^{1+1/n} \right) \right), \\
w_P(x, z, t) &= \frac{S \frac{\partial^2 h}{\partial x^2}}{n+1} \left(1 - S \frac{\partial h}{\partial x}\right)^{1/n-1} A \left( (Y-b)^{1+1/n}(z-b) - \frac{n(Y-b)^{2+1/n}}{2n+1} \right) \\
&- \left(1 - S \frac{\partial h}{\partial x}\right)^{1/n} A \left( \left( \frac{\partial Y}{\partial x} - \frac{\partial b}{\partial x} \right) (Y-b)^{1/n}(z-b) \right) \\
&- \frac{n \frac{\partial Y}{\partial x} (Y-b)^{1+1/n}}{n+1}. \tag{C.5}
\end{aligned}$$

Finally, equations (C.2), (C.4) and (C.5) can be linked by solving for the kinematic boundary condition on the surface  $z = h(x, t)$ , so that

$$\frac{\partial h}{\partial t} + u_P \frac{\partial h}{\partial x} = w_P,$$

giving

$$\frac{\partial h}{\partial t} + A \frac{\partial}{\partial x} \left( \frac{n(Y-b)^{1+1/n}}{(1+n)(1+2n)} \left(1 - S \frac{\partial h}{\partial x}\right)^{1/n} (n(h-Y) + (n+1)(h-b)) \right) = 0. \tag{C.6}$$

- [1] C. Ancey, Plasticity and geophysical flows: A review, *J. Non-Newtonian Fluid Mech.* 142 (2007) 4–35.
- [2] M. E. Eglit, A. E. Yakubenko, Numerical modeling of slope flows entraining bottom material, *Cold Reg. Sci. Technol.* 108 (2014) 139–148.
- [3] D. Issler, Dynamically consistent entrainment laws for depth-averaged avalanche models, *J. Fluid Mech.* 759 (2014) 701–738.
- [4] B. Bouchut, I. R. Ionescu, A. Mangeney, An analytic approach for the evolution of the static/flowing interface in viscoplastic granular flows, *Communications in Mathematical Sciences* in press.
- [5] E. J. Watson, Boundary-layer growth, *Proc. R. Soc. London ser. A* 231 (1955) 104–116.
- [6] P. G. Drazin, N. Riley, *The Navier-Stokes Equations: A classification of Flows and Exact Solutions*, Cambridge University Press, Cambridge, 2006.
- [7] H. Pascal, Propagation of disturbances in a non-Newtonian fluid, *Physica D* 39 (1989) 262–266.
- [8] N. J. Balmforth, Y. Forterre, O. Pouliquen, The viscoplastic Stokes layer, *J. Non-Newtonian Fluid Mech.* 158 (2009) 46–53.
- [9] B. R. Duffy, D. Pritchard, S. K. Wilson, The shear-driven Rayleigh problem for generalised Newtonian fluids, *J. Non-Newtonian Fluid Mech.* 206 (2014) 11–17.
- [10] P. Chadwick, *Continuum Mechanics: Precise Theory and Problems*, Dover, Mineola, 1999.
- [11] L. Fraccarollo, H. Capart, Riemann wave description of erosional dam break flows, *J. Fluid Mech.* 461 (2002) 183–228.
- [12] R. M. Iverson, Elementary theory of bed-sediment entrainment by debris flows and avalanches, *J. Geophys. Res.* 117 (2012) F03006.

- [13] G. Ovarlez, S. Rodts, X. Chateau, P. Coussot, Phenomenology and physical origin of shear localization and shear banding in complex fluids, *Rheol. Acta* 48 (2009) 831–844.
- [14] T. Divoux, M. A. Fardin, S. Manneville, S. Lerouge, Shear banding of complex fluids, *Annu. Rev. Fluid Mech.* 48 (2016) 81–103.
- [15] P. Coussot, Yield stress fluid flows: A review of experimental data, *J. Non-Newtonian Fluid Mech.* 211 (2014) 31–49.
- [16] N. J. Balmforth, I. A. Frigaard, G. Ovarlez, Yielding to Stress: Recent Developments in Viscoplastic Fluid Mechanics, *Annu. Rev. Fluid Mech.* 46 (2014) 121–146.
- [17] G. Ovarlez, Q. Barral, P. Coussot, Three-dimensional jamming and flows of soft glassy materials, *Nature Mater.* 9 (2010) 115–119.
- [18] P. Coussot, Q. D. Nguyen, H. T. Huynh, D. Bonn, Viscosity bifurcation in thixotropic, yielding fluids, *J. Rheol.* 46 (2002) 573–590.
- [19] F. da Cruz, F. Chevoir, D. Bonn, P. Coussot, Viscosity bifurcation in granular materials, foams, and emulsions, *Phys. Rev. E* 66 (2002) 051305.
- [20] P. Møller, A. Fall, V. Chikkadi, D. Derks, D. Bonn, An attempt to categorize yield stress fluid behaviour, *Phil. Trans. Roy. Soc. London A* 367 (2009) 5139–5155.
- [21] G. Picard, A. Ajdari, L. Bocquet, F. Lequeux, Simple model for heterogeneous flows of yield stress fluids, *Phys. Rev. E* 66 (2002) 051501.
- [22] J. Mewis, N. J. Wagner, Thixotropy, *Adv. Colloid Interface Sci.* 147-148 (2009) 214–227.
- [23] G. Ovarlez, S. Rodts, A. Ragouilliaux, P. Coussot, J. Goyon, A. Colin, Wide-gap Couette flows of dense emulsions: Local concentration measurements, and comparison between macroscopic and local constitutive law

- measurements through magnetic resonance imaging, *Phys. Rev. E* 78 (2008) 036307.
- [24] G. Ovarlez, K. Krishan, S. Cohen-Addad, Investigation of shear banding in three-dimensional foams, *EPL* 91 (2010) 68005.
- [25] G. Ovarlez, S. Cohen-Addad, K. Krishan, J. Goyon, P. Coussot, On the existence of a simple yield stress fluid behavior, *J. Non-Newtonian Fluid Mech.* 193 (2013) 68–79.
- [26] O. Thual, L. Lacaze, Fluid boundary of a viscoplastic Bingham flow for finite solid deformations, *J. Non-Newtonian Fluid Mech.* 165 (2010) 84–87.
- [27] P. Saramito, A new elastoviscoplastic model based on the Herschel-Bulkley viscoplastic model, *J. Non-Newtonian Fluid Mech.* 158 (2009) 154–161.
- [28] J. G. Oldroyd, On the formulation of rheological equations of state, *Proc. R. Soc. London ser. A* 200 (1950) 523–541.
- [29] I. Cheddadi, P. Saramito, F. Graner, Steady Couette flows of elastoviscoplastic fluids are nonunique, *J. Rheol.* 56 (2012) 213–239.
- [30] L. Lacaze, A. Filella, O. Thual, Steady and unsteady shear flows of a viscoplastic fluid in a cylindrical Couette cell, *J. Non-Newtonian Fluid Mech.* 220 (2015) 126–136.
- [31] G. Marshall, A front tracking method for one-dimensional moving boundary problems, *SIAM J. Sci. Stat. Comput.* 7 (1986) 252–263.
- [32] K. F. Liu, C. C. Mei, Slow spreading of a sheet of Bingham fluid on an inclined plane, *J. Fluid Mech.* 207 (1990) 505–529.
- [33] C. C. Mei, K. F. Liu, M. Yuhi, Mud flows – Slow and fast, in: N. J. Balmforth, A. Provenzale (Eds.), *Geomorphological Fluid Mechanics: selected topics in geological and geomorphological fluid mechanics*, Springer, Berlin, 548–577, 2001.

- [34] N. J. Balmforth, R. V. Craster, R. Sassi, Shallow viscoplastic flow on an inclined plane, *J. Fluid Mech.* 470 (2002) 1–29.
- [35] N. J. Balmforth, R. V. Craster, A. C. Rust, R. Sassi, Viscoplastic flow over an inclined surface, *J. Non-Newtonian Fluid Mech.* 142 (2007) 219–243.
- [36] C. Ancey, S. Cochard, The dam-break problem for Herschel-Bulkley fluids down steep flumes, *J. Non-Newtonian Fluid Mech.* 158 (2009) 18–35.
- [37] L. Fusi, A. Farina, F. Rosso, Ill posedness of Bingham-type models for the downhill flow of a thin film on an inclined plane, *Quarter. J. App. Math.* 73 (2015) 615–627.
- [38] R. D. Skeel, M. Berzins, A method for the spatial discretization of parabolic equations in one space variable, *SIAM J. Sci. Stat. Comput.* 11 (1990) 1–32.
- [39] B. M. Bates, N. Andreini, C. Ancey, Basal entrainment by Newtonian gravity-driven flows, *Phys. Fluids* 28 (2016) 053101.
- [40] T. Divoux, C. Barentin, S. Manneville, From stress-induced fluidization processes to Herschel-Bulkley behaviour in simple yield stress fluids, *Soft Matter* 7 (2011) 8409–8418.
- [41] T. Divoux, D. Tamarii, C. Barentin, S. Teitel, S. Manneville, Yielding dynamics of a Herschel-Bulkley fluid: a critical-like fluidization behaviour, *Soft Matter* 8 (2012) 4151–4164.
- [42] T. Divoux, D. Tamarii, C. Barentin, S. Manneville, Transient shear banding in a simple yield stress fluid, *Phys. Rev. Lett.* 104 (2010) 208301.
- [43] T. Divoux, C. Barentin, S. Manneville, Stress overshoot in a simple yield stress fluid: An extensive study combining rheology and velocimetry, *Soft Matter* 7 (2011) 9335–9349.
- [44] J. Crank, *The Mathematics of Diffusion*, Oxford University Press, Oxford, 1975.

- [45] R. S. Gupta, D. Kumar, Variable time step methods for one-dimensional Stefan problem with mixed boundary condition, *Int. J. Heat Mass Trans.* 24 (1981) 251–259.
- [46] N. S. Asaithambi, A variable time step Galerkin method for a one-dimensional Stefan problem, *Appl. Math. Comput.* 81 (1997) 189–200.
- [47] S. L. Mitchell, M. Vynnycky, Finite-difference methods with increased accuracy and correct initialization for one-dimensional Stefan problems, *Appl. Math. Comput.* 215 (2009) 1609–1621.
- [48] L. W. Morland, A fixed domain method for diffusion with a moving boundary, *J. Eng. Math.* 16 (1982) 259–269.